INORGANIC CHEMISTRY FRONTIERS

RESEARCH ARTICLE

View Article Online
View Journal | View Issue

Cite this: *Inorg. Chem. Front.*, 2025, **12**, 1900

Deep-ultraviolet sulfamate halides with halogen-centered secondary building units for enhanced optical anisotropy†

Xuefei Wang, [a] Qingwen Zhu,[a] Yunseung Kuk, [b] Hongheng Chen,[c] Qi Wu,*[a] Qun Jing *[c] and Kang Min Ok *[b]

Received 24th December 2024,
Accepted 12th January 2025

DOI: 10.1039/d4qi03302g

rsc.li/frontiers-inorganic

The insufficient birefringence of non-π-conjugated optical materials presents a significant challenge for their deep-ultraviolet (DUV) applications. In this work, four DUV sulfamate halide co-crystals, $AX(NH_3SO_3)$ (A = Rb, Cs; X = Cl, Br), were successfully synthesized through functional chromophore engineering. All four compounds exhibit promising DUV transparent windows, with $RbCl(NH_3SO_3)$ and $CsCl(NH_3SO_3)$ demonstrating short DUV cut-off edges below 185 nm. Remarkably, a significant improvement in birefringence, ranging from 0.069 to 0.075, was observed in all four crystals. These values represent the highest birefringence observed for non-π-conjugated DUV optical materials and exhibit optical anisotropy comparable to that of DUV materials containing π-conjugated groups. Theoretical analysis using the real-space atom-cutting method reveals that the $[XA_m]$ (X = Cl, Br; A = Rb, Cs) secondary building units (SBUs) contribute significantly to the birefringence. The incorporation of halogen-centered chromophores provides a novel strategy for designing non-π-conjugated DUV materials with enhanced birefringence and phase-matching capabilities.

Introduction

Deep-ultraviolet (DUV, $\lambda \leq 200$ nm) optical crystals have been explored for decades, attributable to their birefringent and frequency-doubling capabilities, which arise from their unique anisotropic frameworks.[1,2] Since the emergence of α-BaB_2O_4 (α-BBO) and $KBe_2BO_3F_2$ (KBBF) as excellent short-wavelength birefringent and nonlinear optical (NLO) materials, π-conjugated planar units have been considered ideal for providing optical anisotropy and enhancing birefringence.[3–7] In recent years, more materials featuring π-conjugated $[CO_3]$, $[NO_3]$, $[H_xC_3N_3O_3]$ (x = 1–3), and $[C_6N_7O_3]$ groups have been synthesized as short-wavelength optical materials, offering suitable birefringence for beam splitting or phase matching (PM).[8–12] In contrast, although isotropic tetrahedral units such as $[PO_4]$, $[BO_4]$, and $[SO_4]$ typically exhibit large highest occupied molecular orbital and lowest unoccupied molecular orbital (HOMO–LUMO) gaps and wide transparent windows, the birefringence of non-π-conjugated optical materials composed of alkali or alkaline earth metals is significantly reduced. This is due to the lack of anisotropy in both the cations and anions.[13–16]

Compared to conventional isotropic tetrahedra, their polar tetrahedral variants, such as $[BO_xF_{4-x}]$ (x = 1–3), $[CH_3BF_3]$, $[PO_xF_{4-x}]$ (x = 1–3), $[XSO_3]$ (X = NH_2, NH_3, CH_3, F), which arise from the breaking of T_d symmetry, not only exhibit large HOMO–LUMO gaps but also process higher polarizability anisotropy, hyperpolarizability and enhanced optical anisotropy.[17–24] By employing these polar tetrahedral units, researchers have discovered several materials exhibiting enhanced birefringence ($0.05 \leq \Delta n \leq 0.06$), including $NaNH_4PO_3F{\cdot}H_2O$ (0.053 @ 589.3 nm), *Pc*-$Sr(NH_2SO_3)_2$ (0.056 @ 589.3 nm), and $Cs_2Mg(NH_2SO_3)_4{\cdot}4H_2O$ (0.054 @ 546.1 nm).[23,25,26] These materials show a significant improvement compared to benchmark non-π-conjugated DUV materials with isotropic tetrahedra, such as KH_2PO_4 (KDP, 0.04178 @ 546 nm) and BPO_4 (0.0056 @ 589 nm), offering better PM capacities.[27,28] In the sulfamate system, while the polar $[NH_xSO_3]$ (x = 2, 3) tetrahedra can significantly enhance the anisotropy of crystal frameworks compared to symmetric

[a]*State Key Laboratory of New Textile Materials and Advanced Processing Technologies, Wuhan Textile University, Wuhan 430200, China.*
E-mail: wuqi2011@whu.edu.cn
[b]*Department of Chemistry, Sogang University, Seoul 04107, Republic of Korea.*
E-mail: kmok@sogang.ac.kr
[c]*Xinjiang Key Laboratory of Solid State Physics and Devices, School of Physical Science and Technology, Xinjiang University, Urumqi 830017, China.*
E-mail: qunjing@xju.edu.cn

†Electronic supplementary information (ESI) available: Atomic coordinates, BVS, bond lengths and angles, hydrogen bonds information, analysis on SEM-EDX, elemental analysis, calculations of cation dipole moment, electronic band structures, IR vibrations, and cation coordination in sulfamates. CCDC 2412470–2412473. For ESI and crystallographic data in CIF or other electronic format see DOI: https://doi.org/10.1039/d4qi03302g

anionic groups, the birefringence of sulfamates remains relatively insufficient for optimal DUV PM condition ($0.06 \leq \Delta n \leq 0.08$), limiting their practical applications.[17,29] To enhance the DUV optical performance of metal sulfamates, it is necessary to introduce additional chromophores that can improve birefringence while maintaining a suitable short-wavelength transparent window.

Among all functional units, those with strong electronegativity, such as halogens, have been shown to coordinate with metals to form flexible [XA_m] (X = halogens, A = metals) secondary building units (SBUs), effectively enhancing optical anisotropy. This has been demonstrated by examples such as $[B_6O_{10}]XA_3$ (X = Cl, Br, A = alkali metals), $Ba_3P_3O_{10}X$ (X = Cl, Br), $ABi_2(IO_3)_2F_5$ (A = K, Rb, Cs), and $CsZn_2BO_3X_2$ (X_2 = F_2, Cl_2, FCl).[30–33] Inspired by these findings, it is evident that combining halogen-centered SBUs with polar tetrahedral units can effectively improve the birefringent capabilities of non-π-conjugated materials. Based on the sulfamate system, which has yielded several materials with excellent DUV properties, we successfully combined [XA_m] (X = Cl, Br; A = Rb, Cs) SBUs with [NH_3SO_3] polar tetrahedra to synthesize a series of co-crystals comprising metal halides and sulfamic acid, denoted as AX(NH_3SO_3) (A = Rb, Cs; X = Cl, Br). All four compounds exhibit notably enhanced birefringence, ranging from 0.069 to 0.075, compared to known non-π-conjugated DUV optical materials ($\Delta n \leq 0.056$). Meanwhile, the chloride co-crystals, RbCl(NH_3SO_3) and CsCl(NH_3SO_3), retain excellent DUV cut-off edges below 185 nm.

Experimental section

Reagent and crystal growth

RbCl (Adamas, 99.9%), CsCl (Adamas, 99.9%), RbBr (Adamas, 99.9%), CsBr (Adamas, 99.9%), and sulfamic acid (Fisher chemical, ≥99%) were used as received without further purification. All four crystals, AX(NH_3SO_3) (A = Rb, Cs; X = Cl, Br), were synthesized *via* a room-temperature aqua-solution method using a stoichiometric ratio of 1 : 1 of the corresponding metal halides and sulfamic acid. For example, RbCl(NH_3SO_3) was synthesized by placing RbCl (1 mmol, 0.121 g) and HSO_3NH_2 (1 mmol, 0.097 g) in 10 mL of distilled water in a 20 mL beaker. The mixture was stirred thoroughly to ensure complete reaction. The resulting clear solution was placed in a 30 °C oven for slow evaporation, yielding transparent RbCl(NH_3SO_3) crystals. The other three compounds were synthesized following similar procedures. The yields of the four compounds were calculated based on their respective metals, yielding values of 92.3%, 89.8%, 91.4%, and 94.2% for RbCl(NH_3SO_3), CsCl(NH_3SO_3), RbBr(NH_3SO_3), and CsBr(NH_3SO_3), respectively.

X-ray diffraction analysis

The crystal structures of AX(NH_3SO_3) (A = Rb, Cs; X = Cl, Br) were determined by single crystal X-ray diffraction (SC-XRD) using a BRUKER D8 QUEST diffractometer equipped with monochromatic Mo Kα radiation (λ = 0.71073 Å) at the Advanced Bio-Interface Core Research Facility at Sogang University. Data integration and absorption correction were performed using the SAINT and SCALE programs, respectively.[34] The structural refinement was conducted using the OLEX2 crystallographic software suite.[35] All non-hydrogen atoms were refined *via* full-matrix least-squares techniques. Final least-squares refinement was performed on F_o^2, using data satisfying $F_o^2 \geq 2\sigma(F_o^2)$. Hydrogen atom positions were initially estimated from difference Fourier maps and further optimized through first-principles calculations. Symmetry checks were performed using the PLATON program.[36] Refined crystallographic data are summarized in Table S1.† Bond valence sums (BVS) of all non-H atoms were calculated using the bond valence model developed by Brown.[37] Detailed information, including atomic coordinates, equivalent isotropic displacement parameters, BVS, selected bond lengths and angles, and hydrogen bond distances, is provided in Tables S2-S10 in the ESI.†

Powder X-ray diffraction (PXRD) patterns were collected using a Rigaku MiniFlex 600 diffractometer with Cu Kα radiation (λ = 1.5418 Å). The patterns were recorded over a 5–60° 2θ range with a step size of 0.02° and a scan speed of 7° min^{-1}. Experimental PXRD patterns for AX(NH_3SO_3) (A = Rb, Cs; X = Cl, Br) closely matched their theoretical patterns simulated from SC-XRD data (Fig. S1†).

Spectroscopy

Infrared (IR) spectra were recorded on a Bruker TENSOR 27 ATR-FT-IR spectrometer in the range of 525–4000 cm^{-1}. Ground samples were placed in direct contact with the diamond attenuated total reflectance crystal. The UV-vis diffuse reflectance spectrum was measured at 25 °C using a Lambda 1050 scan UV-vis spectrophotometer, covering the wavelength range of 185–900 nm.

Scanning electron microscopy-energy dispersive analysis by X-ray (SEM-EDX)

SEM-EDX measurements were performed using a JSM-7100F thermal field emission scanning electron microscope equipped with a lens-type ZrO/W Schottky field emission gun. Polycrystalline samples were mounted on carbon tape and coated with platinum prior to analysis. The SEM-EDX results confirmed the presence of Cs, Rb, S, O, N, Cl, and Br in the corresponding compounds, with no other elements detected (Table S11†). These results support the correctness of the structural solutions (Fig. S2†).

Thermogravimetric (TG) analysis

TG analysis was carried out using a SCINCO TGA-N 1000 thermal analyzer. For each measurement, 5–10 mg of ground polycrystalline sample was placed in an alumina crucible and heated under a flow of argon gas from room temperature to 900 °C at a rate of 5 °C min^{-1}.

Birefringence measurement

Birefringence was determined using a ZEISS Axiolab 5 polarized microscope equipped with a 546.1 nm monochromator and a Berek compensator. Retardation (R) was measured for transparent plate-like crystals, with their thickness (d) determined using a BRUKER D8 QUEST diffractometer. The birefringence (Δn) of the selected crystals was calculated using the formula: $R = \Delta n \times d$.

First principles calculations

The electronic structure and linear optical properties were analyzed using the CASTEP package, which adopt a plane-wave pseudopotential method based on density functional theory.[38] The Perdew–Burke–Ernzerhof functional within the generalized gradient approximation framework was employed. The plane wave energy cut-off was set to 830 eV with norm-conserving pseudopotentials to ensure convergence.[39] The valence electronic configurations were specified as follows: Rb: $4s^2 4p^6 5s^1$, Cs: $5s^2 5p^6 6s^1$, S: $3s^2 3p^4$, O: $2s^2 2p^4$, N: $2s^2 2p^3$, Cl: $3s^2 3p^5$, Br: $4s^2 4p^5$, H: $1s^1$. A Monkhorst–Pack grid with k-points in the Brillouin zone was set to $3 \times 2 \times 3$.[40] Other calculation parameters and convergence criteria adhered to the default settings in the CASTEP code. To elucidate the birefringence contributions of each functional unit, the real-space atom-cutting method was employed.[41]

Results and discussion

Crystal structure of $RbCl(NH_3SO_3)$

$RbCl(NH_3SO_3)$ crystallizes in the monoclinic centrosymmetric space group, $P2_1/m$. The asymmetric unit contains one crystallographically independent Rb atom, one Cl atom, one S atom, one N atom, and two O atoms. The Rb1 atoms are coordinated with eight O atoms and two Cl atoms, forming $[RbO_8Cl_2]$ polyhedra (Fig. S3a†). The Rb–O bond lengths range from 2.9556(13) to 3.1891(14) Å, while the Rb–Cl bond length is 3.4336(7) Å. The S atoms are coordinated with three O atoms and one N atom, forming $[NSO_3]$ tetrahedra. The S–O bond lengths vary from 1.4345(13) to 1.4383(19) Å, and the S–N bond length is 1.759(2) Å. Due to the distinct electronic environments of amine and ammonia groups, the S–N bond lengths in $[NSO_3]$ tetrahedra differ significantly between $[NH_2SO_3]$ and $[NH_3SO_3]$ configurations. Based on previously reported sulfamates and sulfamic acid co-crystals, the S–N bond lengths range from 1.62 Å to 1.64 Å for $[NH_2SO_3]$ units and from 1.74 Å to 1.76 Å for $[NH_3SO_3]$ units. Therefore, the compound is identified as a co-crystal comprising RbCl and sulfamic acid. Similarly, $CsCl(NH_3SO_3)$, $RbBr(NH_3SO_3)$, and $CsBr(NH_3SO_3)$ were determined to be co-crystals of sulfamic acid and their respective metal halides, following the same bond-length principles for S–N bonds.

$RbCl(NH_3SO_3)$ exhibits a characteristic two-dimensional (2D) layered structure, with the layers stacking along the c-axis (Fig. 1a). The $[NH_3SO_3]$ molecules adopt an anti-parallel

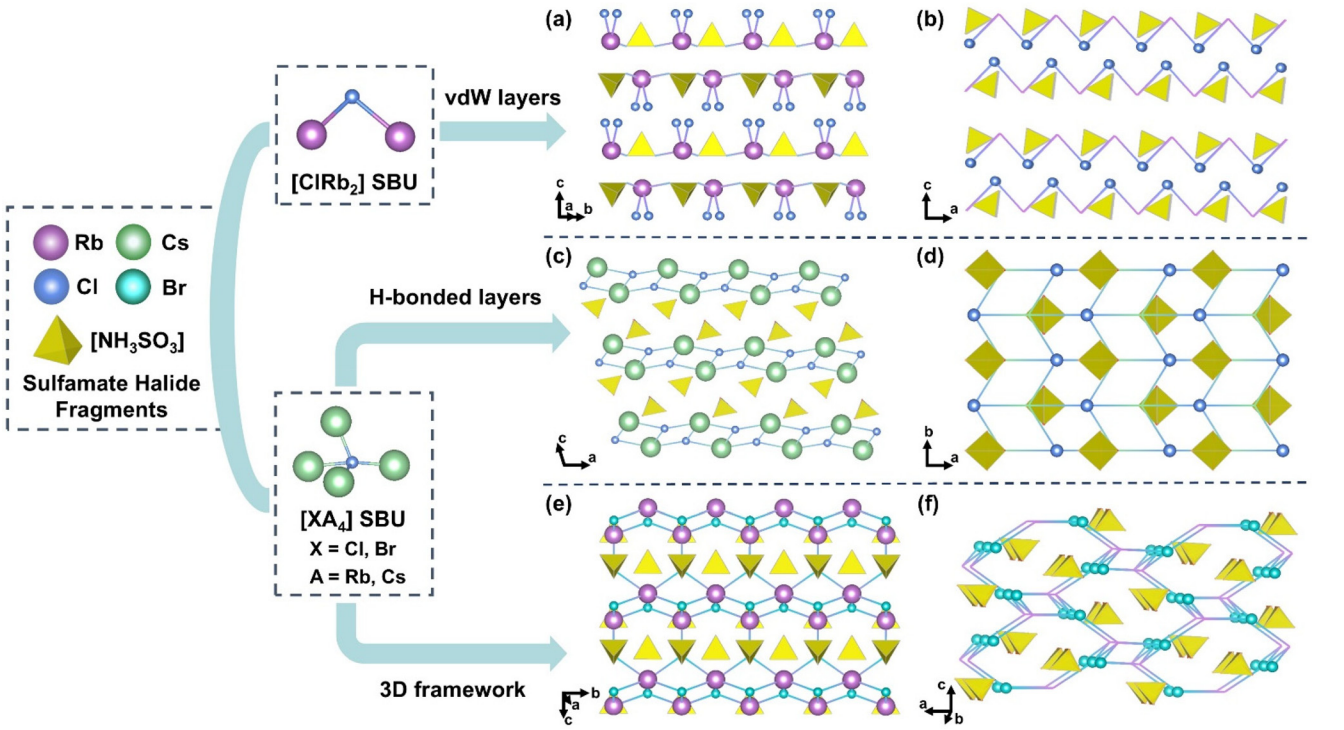

Fig. 1 (a) The 2D vdW layers of $RbCl(NH_3SO_3)$ viewed perpendicular to the c-axis. (b) The infinite $[ClRb]_\infty$ 1D chains in $RbCl(NH_3SO_3)$ viewed along the b-axis. (c) The layered structure of $CsCl(NH_3SO_3)$ viewed along the a-axis. (d) The 2D $[ClRb]_\infty$ layers in $CsCl(NH_3SO_3)$ viewed along the c-axis. (e) The 3D halogen-metal framework of $RbBr(NH_3SO_3)$ viewed along the pseudo-layered direction. (f) The 3D halogen-metal framework of $RbBr(NH_3SO_3)$ viewed perpendicular to the pseudo-layered direction.

arrangement due to the symmetric operation of the 2/*m* point group. Adjacent Rb1 atoms coordinate with the oxygen atoms of the $[NH_3SO_3]$ molecules through corner- and edge-sharing, forming a pseudo-double layer along the *ab* planes (Fig. S3b†). Due to the strong electronegativity of Cl atoms, the Cl1 atoms are displaced from the pseudo-layers and bridge two Rb atoms, forming $[ClRb_2]$ SBUs. These SBUs further create infinite $[ClRb]_\infty$ 1D chains along the *a*-axis, which are alternately arranged with $[NH_3SO_3]$ molecules in the *ab* plane (Fig. 1b). The BVS calculations and the donor–acceptor distance between Cl1 and N1 atoms suggest that Cl1 acts as a hydrogen bond acceptor from the $[NH_3SO_3]$ molecules. The donor–acceptor distances range from 3.2049(7) to 3.214(2) Å. As no typical chemical bonds exist between adjacent layers, RbCl(NH_3SO_3) is classified as a layered molecular crystal, held together by van der Waals (vdW) forces.

Crystal structure of CsCl(NH_3SO_3)

CsCl(NH_3SO_3) crystallizes in the $P2_1/m$ space group. however, the material exhibits a structure distinct from RbCl(NH_3SO_3) attributed to the larger ionic radius of Cs^+. The asymmetric unit consists of one Cs atom, one Cl atom, one S atom, one N atom, and two O atoms. The Cs1 atom is coordinated with seven O atoms and four Cl atoms, forming $[CsO_7Cl_4]$ polyhedra (Fig. S4a†). The Cs–O bond lengths range from 3.1135(17) to 3.534(3) Å, while the Cs–Cl bond lengths vary from 3.5808(17) to 3.6759(11) Å. The $[NH_3SO_3]$ molecules adopt an anti-parallel arrangement and coordinate with the Cs1 atoms through corner- and edge-sharing, creating a 2D pseudo-layer along the *ab* plane (Fig. 1c). Due to the difference in ionic radii between Cs^+ and Rb^+, the coordination environment of the Cl1 atom in CsCl(NH_3SO_3) differs significantly from the 2-coordinated Cl atoms in RbCl(NH_3SO_3). In CsCl(NH_3SO_3), the Cl1 atom coordinates with four Cs atoms, forming $[ClCs_4]$ SBUs. These SBUs assemble into infinite 2D $[ClCs]_\infty$ layers extending within the *ab* plane, oriented perpendicular to the pseudo-layer formed by the sulfamic acid molecules (Fig. 1d). Consequently, adjacent layers are linked by weak Cs–Cl and Cs–O ionic interactions, in contrast to the vdW forces observed in RbCl(NH_3SO_3).

Crystal structures of RbBr(NH_3SO_3) and CsBr(NH_3SO_3)

Both RbBr(NH_3SO_3) and CsBr(NH_3SO_3) crystallize in the orthorhombic *Pnma* space group, sharing an isostructural framework and similar cationic coordination environments. The slight differences in unit cell parameters along the *a*- and *c*-axes arise from the variation in ionic radii between Rb^+ and Cs^+. The asymmetric unit of RbBr(NH_3SO_3) comprises one Rb atom, one Br atom, one S atom, one N atom, and two O atoms, while in CsBr(NH_3SO_3), the Rb atom is replaced by a Cs atom (Fig. S4b†). The $[RbO_7Br_4]$ ($[CsO_7Br_4]$) polyhedra are formed by the coordination of the Rb1 (Cs1) atom with seven O atoms and four Br atoms. The bond distances for Rb–O and Cs–O are 3.025(2)–3.2141(13) Å and 3.224(4)–3.315(4) Å, respectively, while the Rb–Br and Cs–Br bond distances are 3.6459(10)–3.7213(9) Å and 3.7390(7)–3.9088(11) Å, respectively. The Br atoms in RbBr(NH_3SO_3) and CsBr(NH_3SO_3) coordinate with four Rb (or Cs) atoms, forming the $[BrRb_4]$ ($[BrCs_4]$) SBUs (Fig. 1e). Unlike CsCl(NH_3SO_3), the incorporation of larger Br^- ions leads to SBUs with higher connectivity, resulting in 3D $[BrRb]_\infty$ ($[BrCs]_\infty$) halogen-metal frameworks (Fig. 1f). The longer Rb–Br and Cs–Br bond distances and the looser framework structures cause the $[NH_3SO_3]$ molecules to intersect at angles of 115.7(1)° and 120.5(4)°, rather than adopting the antiparallel arrangement seen in CsCl(NH_3SO_3) (Fig. S5†). These differences in molecular arrangements highlight the flexibility of halogen-metal frameworks and suggest a promising approach for regulating the arrangement of neutral or anionic groups to achieve desirable properties.

Thermal analysis

TG analysis was conducted to assess the thermal stability of the four compounds (Fig. S6†). All four compounds exhibit similar thermal stability up to approximately 142 °C. Beyond this temperature, gradual weight losses were observed between 142 and 800 °C, attributed to the decomposition of sulfamic acid and halogens. At 800 °C, the observed residual weights for CsCl(NH_3SO_3) and CsBr(NH_3SO_3) are 73.01% and 61.97%, respectively, which closely align with the calculated values of 68.30% and 58.41% based on the decomposition products of Cs_2SO_4. Similarly, RbCl(NH_3SO_3) and RbBr(NH_3SO_3) exhibit residual weights of 68.41% and 58.12%, respectively, which are slightly higher than the calculated values of 61.51% and 50.86% based on the decomposition products of Rb_2SO_4. These discrepancies may be attributed to incomplete decomposition of the compounds. Theoretical and experimental weight loss data are provided in the ESI (Table S12†).

IR and UV-vis spectroscopic analysis

IR spectra of the four compounds, recorded in the range of 4000–400 cm^{-1}, were analyzed to identify their functional groups (Fig. S7†). The characteristic peaks of RbCl(NH_3SO_3) are described as representative due to the similarity in vibrational features across all four compounds. Peaks at 1265, 1060, 978, and 691 cm^{-1} are attributed to the anti-symmetric and symmetric stretching vibrations of the S–O interactions in the $[NH_3SO_3]$ groups. Absorption peaks in the ranges of 1410–1425 cm^{-1}, 2430–2440 cm^{-1}, and 3160–3210 cm^{-1} correspond to the bending, wagging, and stretching vibrations of the $[NH_3]$ units, respectively. The assigned peaks for all four compounds are consistent with previously reported experimental and theoretical IR data for sulfamates (Table S13†).[23]

The UV-vis diffuse reflectance spectra were measured to determine the UV transparent windows of the four compounds. As shown in Fig. 2a and b, RbCl(NH_3SO_3) and CsCl(NH_3SO_3) exhibit high reflectance from the visible light region to the DUV range, with reflectance values of 85.26% and 46.40% at 185 nm, respectively. These results indicate wide DUV transparent windows. In contrast, the presence of Br^- anions cause a red-shift in the cut-off edges of RbBr(NH_3SO_3) and CsBr(NH_3SO_3) to 193 nm and 195 nm, respectively (Fig. 2c and d). The optical band gaps of the compounds were esti-

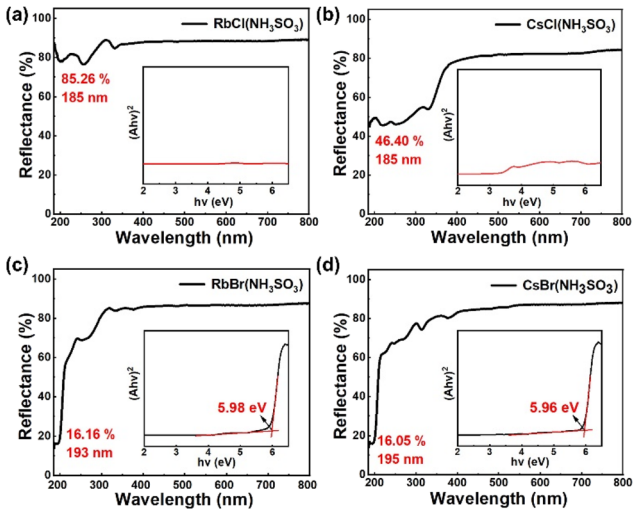

Fig. 2 UV-vis diffuse reflectance spectra of (a) $RbCl(NH_3SO_3)$, (b) $CsCl(NH_3SO_3)$, (c) $RbBr(NH_3SO_3)$, and (d) $CsBr(NH_3SO_3)$.

mated using the Kubelka–Munk function. The calculated band gaps are >6.70 eV for $RbCl(NH_3SO_3)$ and $CsCl(NH_3SO_3)$, 5.98 eV for $RbBr(NH_3SO_3)$, and 5.96 eV for $CsBr(NH_3SO_3)$. These results demonstrate that the introduction of halides maintains wide UV and DUV transparent windows while only slightly reducing the bandgaps compared to metal sulfamates.

Electronic structures

First-principles calculations were performed to analyze the electronic band structures and the total and partial density of states (DOS) of the four compounds. The results reveal that the valence band maximum and conduction band minimum for all four compounds are located at the Γ point, indicating direct band gaps of 4.584, 4.607, 4.217, and 4.233 eV for $RbCl(NH_3SO_3)$, $CsCl(NH_3SO_3)$, $RbBr(NH_3SO_3)$, and $CsBr(NH_3SO_3)$, respectively (Fig. S8†). An analysis of the total and partial DOS shows that the tops of the valence bands are primarily dominated by Cl-3p and Br-4p orbitals. In contrast, the bottoms of the conduction bands consist of hybridized s and p orbitals from Rb, Cs, S, O, and N atoms, depending on the specific compound. These results suggest that the band gaps of these compounds are predominantly influenced by A–X (A = Rb, Cs; X = Cl, Br) interactions (Fig. 3).

Birefringence and contributions of halogen-centered SBUs

The birefringence of the four compounds was quantitatively determined by measuring the wavelength retardation of the crystals using a Berek compensator. Plate-like crystals with thicknesses of 12.079 μm for $RbCl(NH_3SO_3)$, 17.443 μm for $CsCl(NH_3SO_3)$, 9.977 μm for $RbBr(NH_3SO_3)$, and 6.662 μm for $CsBr(NH_3SO_3)$ were used in the measurements. The recorded retardations were 843.9, 1277.3, 719.28, and 449.72 nm, corresponding to birefringence values of 0.069, 0.073, 0.072, and 0.075 at 546.1 nm, respectively (Fig. 4a–d).

The frequency-dependent birefringence of the four compounds was estimated using first principles calculations (Fig. 4e–h). Due to the typical underestimation of band gaps by the generalized gradient approximation used in the exchange–correlation energy functional, scissor operators of 1.763 eV and 1.727 eV were applied to correct the refractive index calculations for $RbBr(NH_3SO_3)$ and $CsBr(NH_3SO_3)$, based on their experimental band gaps. For $RbCl(NH_3SO_3)$ and $CsCl(NH_3SO_3)$, the band gaps were calculated using the HSE06 hybrid functional, yielding values of 6.942 eV and 6.923 eV, respectively. Corresponding scissor operators of 2.358 eV and 2.316 eV were applied for corrections. The estimated birefringence values at 532 nm were 0.065, 0.066, 0.071, and 0.064 for $RbCl(NH_3SO_3)$, $CsCl(NH_3SO_3)$, $RbBr(NH_3SO_3)$, and $CsBr(NH_3SO_3)$, respectively. These values are consistent with the experimental results at 546.1 nm, confirming the birefringence enhancement in non-π-conjugated system.

To elucidate the origin of enhanced birefringence in sulfamate halide co-crystals, the real-space atom-cutting method, based on theoretically calculated refractive indices, was employed to analyze the birefringence contributions of each functional unit. Since the structures of the four compounds comprise isolated covalent molecules and metal–halide ionic frameworks, they were divided into sulfamic acid molecules

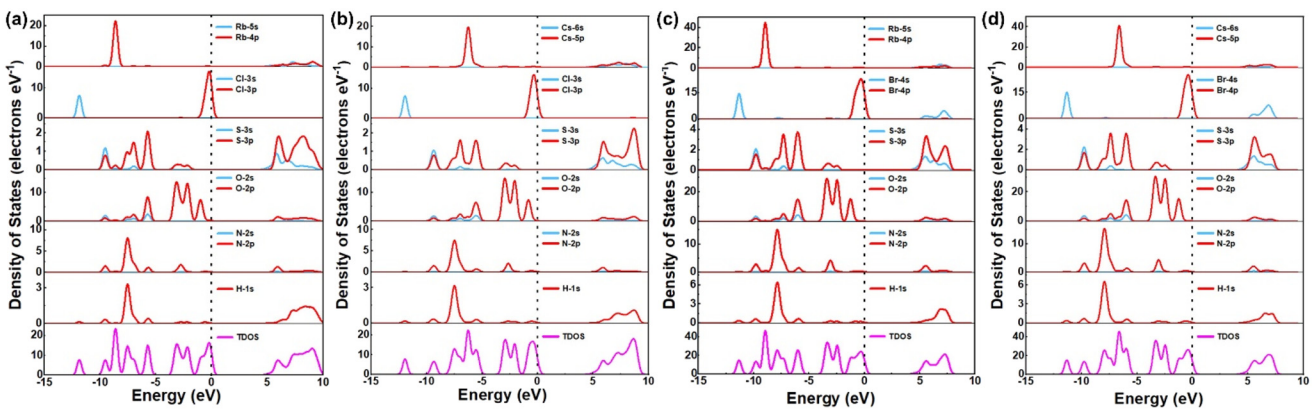

Fig. 3 Total and partial DOS of (a) $RbCl(NH_3SO_3)$, (b) $CsCl(NH_3SO_3)$, (c) $RbBr(NH_3SO_3)$, and (d) $CsBr(NH_3SO_3)$.

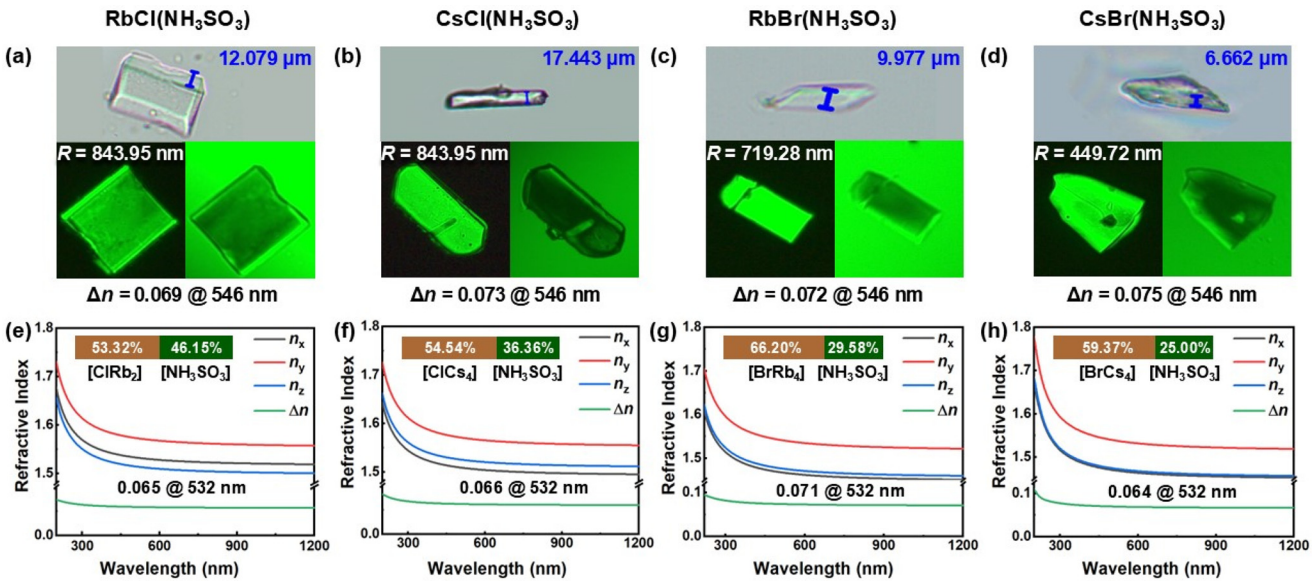

Fig. 4 Measured birefringence at 546.1 nm of (a) $RbCl(NH_3SO_3)$, (b) $CsCl(NH_3SO_3)$, (c) $RbBr(NH_3SO_3)$, and (d) $CsBr(NH_3SO_3)$. Calculated frequency-dependent refractive indices and birefringence of (e) $RbCl(NH_3SO_3)$, (f) $CsCl(NH_3SO_3)$, (g) $RbBr(NH_3SO_3)$, and (h) $CsBr(NH_3SO_3)$. Insets of (e)–(h) show the birefringence contributions of halogen-centered SBUs and sulfamic acid polar tetrahedral groups, as calculated using the real-space atom-cutting method.

and halogen-centered SBUs, specifically $[ClRb_2]$, $[ClCs_4]$, $[BrRb_4]$, and $[BrCs_4]$ in the respective compounds. Due to approximations made near the edges of electron clouds when estimating the spatial contributions of atomic or ionic groups, the sum of birefringence contributions from each unit may not strictly equal 100%. However, this discrepancy does not affect the scientific conclusions. The $[XA_m]$ (X = Cl, Br; A = Rb, Cs) SBUs make substantial contributions to birefringence, specifically 52.31% and 54.54% for $RbCl(NH_3SO_3)$ and $CsCl(NH_3SO_3)$, and dominantly 66.20% and 59.37% for $RbBr(NH_3SO_3)$ and $CsBr(NH_3SO_3)$, respectively. These results indicate that introducing halogens enhances optical anisotropy while providing an effective strategy to improve DUV phase-matching capabilities in potential noncentrosymmetric metal sulfamate halides.

To validate this improvement, a statistical analysis of cut-off edges and birefringence values for UV and DUV optical materials composed exclusively of non-π-conjugated functional units – including phosphates, sulfates, sulfamates, and other tetrahedral structures was performed (Fig. 5 and Table S14†). Non-π-conjugated functional units typically exhibit limited microscopic optical anisotropy. Consequently, most DUV phosphates and sulfates containing alkali or alkaline earth metals have relatively low birefringence, typically ranging from 0 to 0.05. Materials featuring stereochemically active metals, such as Bi^{3+} and Sb^{3+}, or S–S tetrahedral overlap achieve higher birefringence but suffer from noticeable red-shift in their cut-off edges, often exceeding 230 nm. While sulfamates and other polar non-π-conjugated tetrahedra show improved birefringence compared to phosphates and sulfates, achieving optimal phase-matching birefringence in the range of 0.06–0.08 with suitable DUV cut-off edges remains a challenge. The four sulfamate halide co-crystals stand out by combining large birefringence with wide DUV-transparent windows, underscoring the effectiveness of integrating halogen-centered SBUs with polar tetrahedra. Notably, the birefringence values of $RbCl(NH_3SO_3)$ and $CsCl(NH_3SO_3)$ exceed the previously established ceiling for DUV non-π-conjugated optical materials (0.056 @ 589.3 nm for *Pc*-$Sr(NH_2SO_3)_2$) while avoiding red-shifts in their cut-off edges.[17] Moreover, the birefringence values are comparable to

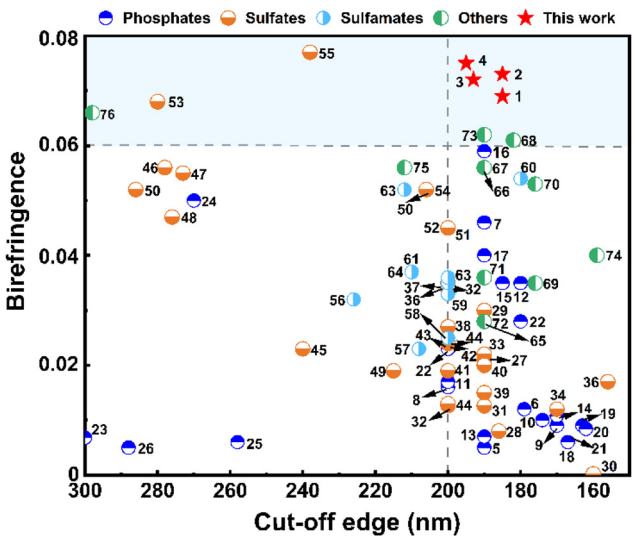

Fig. 5 Comparison of non-π-conjugated optical materials derivatives in the UV and DUV regions.

those of optical materials with π-conjugated functional groups, such as KBBF (0.077 @ 1064 nm), $BaB_4O_6F_2$ (0.065 @ 400 nm), $Sr_2NO_3(OH)_3$ (0.076 @ 532 nm), $Na_2Ca_2(CO_3)_3$ (0.061 @ 1064 nm), $Y_8O(OH)_{15}(CO_3)_3Cl$ (0.045 @ 1064 nm).[42–46]

Conclusions

In summary, the first four DUV sulfamate halide co-crystals, $AX(NH_3SO_3)$ (A = Rb, Cs; X = Cl, Br), were successfully synthesized using a room-temperature aqua-solution method. The introduction of Cl^- and Br^- anions has a minimal impact on the short-wavelength transparent window. Specifically, the chloride co-crystals, $RbCl(NH_3SO_3)$ and $CsCl(NH_3SO_3)$, exhibit short DUV cut-off edges below 185 nm. Remarkably, the four crystals display improved birefringence values in the range of 0.069–0.075, as determined using a polarized microscope. These values are comparable to those of DUV materials featuring π-conjugated groups. Theoretical analysis employing the real-space atom-cutting method reveals that the $[XA_m]$ (X = Cl, Br, A = Rb, Cs) SBUs contribute significantly to the optical anisotropy and birefringence. These findings not only demonstrate that sulfamate halides are a promising system for developing DUV optical materials but also provide a novel approach for designing non-π-conjugated DUV materials with enhanced birefringence and phase-matching capabilities.

Data availability

Data available on request from the authors.

The data that support the findings of this study are available from the corresponding authors, KMO, QJ, or QW upon reasonable request.

Conflicts of interest

There are no conflicts to declare.

Acknowledgements

This research was supported by the National Natural Science Foundation of China (22405197 and 22275052) and the Tianshan Talent Training Program of Xinjiang Uygur Autonomous Region of China (2022TSYCJU0004). This research was also supported by the National Research Foundation of Korea (NRF) funded by the Ministry of Science and ICT (Grant No. RS-2024-00442105).

References

1 Y. Wang, B. Zhang, Z. Yang and S. Pan, Cation-Tuned Synthesis of Fluorooxoborates: Towards Optimal Deep-Ultraviolet Nonlinear Optical Materials, *Angew. Chem., Int. Ed.*, 2018, **57**, 2150–2154.

2 C. Wu, C. Jiang, G. Wei, X. Jiang, Z. Wang, Z. Lin, Z. Huang, M. G. Humphrey and C. Zhang, Toward Large Second-Harmonic Generation and Deep-UV Transparency in Strongly Electropositive Transition Metal Sulfates, *J. Am. Chem. Soc.*, 2023, **145**, 3034–3046.

3 C. T. Chen, G. L. Wang, X. Y. Wang and Z. Y. Xu, Deep-UV Nonlinear Optical Crystal $KBe_2BO_3F_2$—Discovery, Growth, Optical Properties and Applications, *Appl. Phys. B*, 2009, **97**, 9–25.

4 D. Cyranoski, China's Crystal Cache: a Chinese Laboratory is the Only Source of a Valuable Crystal. David Cyranoski Investigates Why It Won't Share Its Supplies, *Nature*, 2009, **457**, 953–956.

5 G. Zhou, J. Xu, X. Chen, H. Zhong, S. Wang, K. Xu, P. Deng and F. Gan, Growth and Spectrum of a Novel Birefringent α-BaB_2O_4 Crystal, *J. Cryst. Growth*, 1998, **191**, 517–519.

6 Y. Liu, Y. Shen, S. Zhao and J. Luo, Structure-property Relationship in Nonlinear Optical Materials with π-conjugated CO_3 Triangles, *Coord. Chem. Rev.*, 2020, **407**, 20.

7 W. Zhang, X. Hou, S. Han and S. Pan, Toward the Ultraviolet (UV) or Deep-UV Nonlinear Optical Crystals: The Combination of π-conjugated Planar $[XY_3]$ and Tetrahedral $[XY_4]$, *Coord. Chem. Rev.*, 2024, **505**, 31.

8 X. Hao, M. Luo, C. Lin, G. Peng, T. Yan, D. Lin, L. Cao, X. Long, G. Yang and N. Ye, $A(H_3C_3N_3O_3)(NO_3)$ (A = K, Rb): Alkali-metal Nitrate Isocyanurates with Strong Optical Anisotropy, *Inorg. Chem.*, 2020, **59**, 10361–10367.

9 X. Liu, L. Kang, P. Gong and Z. Lin, $LiZn(OH)CO_3$: A Deep-Ultraviolet Nonlinear Optical Hydroxycarbonate Designed from a Diamond-like Structure, *Angew. Chem., Int. Ed.*, 2021, **60**, 13574–13578.

10 X. Meng, K. Kang, F. Liang, J. Tang, W. Yin, Z. Lin and M. Xia, Optimal Arrangement of π-conjugated Anionic Groups in Hydro-isocyanurates Leads to Large Optical Anisotropy and Second-harmonic Generation Effect, *Inorg. Chem. Front.*, 2020, **7**, 3674–3686.

11 C. Wu, X. Jiang, Z. Wang, L. Lin, Z. Lin, Z. Huang, X. Long, M. G. Humphrey and C. Zhang, Giant Optical Anisotropy in the UV-transparent 2D Nonlinear Optical Material $Sc(IO_3)_2(NO_3)$, *Angew. Chem., Int. Ed.*, 2021, **60**, 3464–3648.

12 X. Zhang, X. Du, J. Wang, F. Wang, F. Liang, Z. Hu, Z. Lin and Y. Wu, $K_3C_6N_7O_3{\cdot}2H_2O$: A Multifunctional Nonlinear Optical Cyamelurate Crystal with Colossal π-conjugated Orbitals, *ACS Appl. Mater. Interfaces*, 2022, **14**, 53074–53080.

13 L. Kang, P. Gong, Z. Lin and B. Huang, Deep-Ultraviolet Nonlinear-Optical van der Waals Beryllium Borates, *Angew. Chem., Int. Ed.*, 2021, **60**, 16680–16686.

14 S. Liu, X. Jiang, L. Qi, Y. Hu, K. Duanmu, C. Wu, Z. Lin, Z. Huang, M. G. Humphrey and C. Zhang, An Unprecedented $[BO_2]$-Based Deep-Ultraviolet Transparent Nonlinear Optical Crystal by Superhalogen Substitution, *Angew. Chem., Int. Ed.*, 2024, **63**, e202403328.

15 T. Wu, X. Jiang, C. Wu, Z. Lin, Z. Huang, M. G. Humphrey and C. Zhang, $Ce_3F_4(SO_4)_4$: Cationic Framework Assembly for Designing Polar Nonlinear Optical Material through Fluorination Degree Modulation, *Inorg. Chem. Front.*, 2023, **10**, 5270–5277.

16 S. Zhao, P. Gong, S. Luo, L. Bai, Z. Lin, C. Ji, T. Chen, M. Hong and J. Luo, Deep-ultraviolet Transparent Phosphates $RbBa_2(PO_3)_5$ and $Rb_2Ba_3(P_2O_7)_2$ Show Nonlinear Optical Activity from Condensation of $[PO_4]^{3-}$ units, *J. Am. Chem. Soc.*, 2014, **136**, 8560–8563.

17 D. Dou, Q. Shi, H. Li, B. Zhang and Y. Wang, Rational Combination of π–Conjugated and Non-π-Conjugated Groups Achieving Strong Nonlinear Optical Response, Large Optical Anisotropy, and UV Light–Switchable Fluorescence, *Adv. Sci.*, 2024, **11**, 2401325.

18 W. Jin, C. Xie, X. Hou, M. Cheng, E. Tikhonov, M. Wu, S. Pan and Z. Yang, From Monofluorophosphates A_2PO_3F to Difluorophosphates APO_2F_2 (A = alkali metal): Design of a Potential Deep-ultraviolet Nonlinear Optical Materials System with a Shortened Phase-matching Wavelength, *Chem. Mater.*, 2023, **35**, 5281–5290.

19 K. Liu, J. Han, T. Baiheti, F. Li, Z. Wei, Z. Yang, M. Mutailipu and S. Pan, Finding a Series of $BaBOF_3$ Fluorooxoborate Polymorphs with Tunable Symmetries: A Simple but Flexible Case, *Chem. Mater.*, 2021, **33**, 7905–7913.

20 M. Mutailipu, K. R. Poeppelmeier and S. Pan, Borates: A Rich Source for Optical Materials, *Chem. Rev.*, 2020, **121**, 1130–1202.

21 H. Qiu, F. Li, C. Jin, Z. Yang, J. Li, S. Pan and M. Mutailipu, Fluorination Strategy Towards Symmetry Breaking of Boron-centered Tetrahedron for Poly-fluorinated Optical Crystals, *Angew. Chem., Int. Ed.*, 2024, **63**, e202316194.

22 D. Dou, Q. Shi, Y. Bai, C. Chen, B. Zhang and Y. Wang, $C_3N_6H_7SO_3NH_2$: Non-π-conjugated Tetrahedra Decoupling π-conjugated Groups Achieving Large Optical Anisotropy and Wide Band Gap, *Mater. Chem. Front.*, 2023, **7**, 5924–5931.

23 X. Wang, X. Leng, Y. Kuk, J. Lee, Q. Jing and K. M. Ok, Deep-Ultraviolet Transparent Mixed Metal Sulfamates with Enhanced Nonlinear Optical Properties and Birefringence, *Angew. Chem., Int. Ed.*, 2024, **63**, e202315434.

24 L. Xiong, J. Chen, J. Lu, C.-Y. Pan and L.-M. Wu, Monofluorophosphates: a New Source of Deep-ultraviolet Nonlinear Optical Materials, *Chem. Mater.*, 2018, **30**, 7823–7830.

25 P. Gross, Y. Zhang, L. Bayarjargal, B. Winkler and H. A. Höppe, New Alkaline-earth Amidosulfates and Their Unexpected Decomposition to S_4N_4, *Dalton Trans.*, 2022, **51**, 11737–11746.

26 J. Lu, J.-N. Yue, L. Xiong, W.-K. Zhang, L. Chen and L.-M. Wu, Uniform Alignment of Non-π-conjugated Species Enhances Deep Ultraviolet Optical Nonlinearity, *J. Am. Chem. Soc.*, 2019, **141**, 8093–8097.

27 X. Zhang, L. Wang, S. Zhang, G. Wang, S. Zhao, Y. Zhu, Y. Wu and C. Chen, Optical Properties of the Vacuum-ultraviolet Nonlinear Optical Crystal-BPO_4, *J. Opt. Sos. Am. B*, 2011, **28**, 2236–2239.

28 L. Zhu, X. Zhang, M. Xu, B. Liu, S. Ji, L. Zhang, H. Zhou, F. Liu, Z. Wang and X. Sun, Refractive Indices in the Whole Transmission Range of Partially Deuterated KDP Crystals, *AIP Adv.*, 2013, **3**, 112114.

29 D. Dou, B. Cai, B. Zhang and Y. Wang, $M(NH_2SO_3)_2{\cdot}xH_2O$ (M = Ca, Pb, x = 0, 1, 4): Effect of Hydrogen Bonding on Structural Transformations and Second Harmonic Generation of Metal Sulfamates, *Inorg. Chem.*, 2022, **61**, 21131–21138.

30 H. Liu, Q. Wu, X. Jiang, Z. Lin, X. Meng, X. Chen and J. Qin, $ABi_2(IO_3)_2F_5$ (A = K, Rb, and Cs): A Combination of Halide and Oxide Anionic Units To Create a Large Second-Harmonic Generation Response with a Wide Bandgap, *Angew. Chem., Int. Ed.*, 2017, **56**, 9492–9496.

31 Z. Yang, B.-H. Lei, B. Yang and S. Pan, "XA_6" Octahedra Influencing the Arrangement of Anionic Groups and Optical Properties in Inverse-perovskite $[B_6O_{10}]XA_3$ (X = Cl, Br; A = Alkali Metal), *Phys. Chem. Chem. Phys.*, 2016, **18**, 15394–15398.

32 P. Yu, L.-M. Wu, L.-J. Zhou and L. Chen, Deep-ultraviolet Nonlinear Optical Crystals: $Ba_3P_3O_{10}X$ (X = Cl, Br), *J. Am. Chem. Soc.*, 2014, **136**, 480–487.

33 J. Zhou, Y. Liu, H. Wu, H. Yu, Z. Lin, Z. Hu, J. Wang and Y. Wu, $CsZn_2BO_3X_2$ (X_2 = F_2, Cl_2, and FCl): A Series of Beryllium-Free Deep-Ultraviolet Nonlinear-Optical Crystals with Excellent Properties, *Angew. Chem., Int. Ed.*, 2020, **59**, 19006–19010.

34 SAINT, A 7.60, Bruker Analytical X-ray Instruments, Inc., Madison, WI, 2008.

35 O. V. Dolomanov, L. J. Bourhis, R. J. Gildea, J. A. Howard and H. Puschmann, OLEX2: a Complete Structure Solution, Refinement and Analysis Program, *J. Appl. Crystallogr.*, 2009, **42**, 339–341.

36 A. Spek, Single-crystal Structure Validation with the Program PLATON, *J. Appl. Crystallogr.*, 2003, **36**, 7–13.

37 I. D. Brown, Recent Developments in the Methods and Applications of the Bond Valence Model, *Chem. Rev.*, 2009, **109**, 6858–6919.

38 V. Milman, K. Refson, S. Clark, C. Pickard, J. Yates, S. P. Gao, P. Hasnip, M. Probert, A. Perlov and M. Segall, Electron and Vibrational Spectroscopies Using DFT, Plane Waves and Pseudopotentials: CASTEP Implementation, *J. Mol. Struct.*, 2010, **954**, 22–35.

39 J. P. Perdew and Y. Wang, Pair-distribution Function and Its Coupling-constant Average for the Spin-polarized Electron Gas, *Phys. Rev. B:Condens. Matter Mater. Phys.*, 1992, **46**, 12947.

40 P. Wisesa, K. A. McGill and T. Mueller, Efficient Generation of Generalized Monkhorst-Pack Grids through the Use of Informatics, *Phys. Rev. B*, 2016, **93**, 155109.

41 J. Lin, M. H. Lee, Z. P. Liu, C. Chen and C. Pickard, Mechanism for Linear and Nonlinear Optical Effects in β-BaB_2O_4 Crystals, *Phys. Rev. B:Condens. Matter Mater. Phys.*, 1999, **60**, 13380.

42 B. Wu, D. Tang, N. Ye and C. Chen, Linear and Nonlinear Optical Properties of the $KBe_2BO_3F_2$ (KBBF) Crystal, *Opt. Mater.*, 1996, **5**, 105–109.
43 Z. Zhang, Y. Wang, B. Zhang, Z. Yang and S. Pan, Designing Deep-UV Birefringent Crystals by Cation Regulation, *Chem. – Eur. J.*, 2018, **24**, 11267–11272.
44 L. Huang, G. Zou, H. Cai, S. Wang, C. Lin and N. Ye, $Sr_2(OH)_3NO_3$: the First Nitrate as a Deep UV Nonlinear Optical Material with Large SHG Responses, *J. Mater. Chem. C*, 2015, **3**, 5268–5274.
45 Y. Song, M. Luo, D. Zhao, G. Peng, C. Lin and N. Ye, Explorations of New UV Nonlinear Optical Materials in the Na_2 CO_3-$CaCO_3$ System, *J. Mater. Chem. C*, 2017, **5**, 8758–8764.
46 Y. Zhang, Y. Long, X. Dong, L. Wang, L. Huang, H. Zeng, Z. Lin, X. Wang and G. Zou, $Y_8O(OH)_{15}(CO_3)_3Cl$: an excellent short-wave UV nonlinear optical material exhibiting an infrequent three-dimensional inorganic cationic framework, *Chem. Commun.*, 2019, **55**, 4538–4541.